This document is the **Accepted Manuscript** version of a Published Work that appeared in final form in: *Journal of Physical Chemistry C : Nanomaterials and Interfaces*, 2021, 125, 48, 26645–26651, Copyright © American Chemical Society after peer review and technical editing by the publisher. To access the final edited and published work see https://doi.org/10.1021/acs.jpcc.1c08594

# Signatures of Dichalcogenide-Gold Interaction in the Vibrational Spectra of $MoS_2$ and $MoSe_2$ on Au(111)

Soumyajit Sarkar and Peter Kratzer*

*Fakultät für Physik, Universität Duisburg-Essen, Campus Duisburg, Lotharstr. 1, 47057 Duisburg, Germany*

E-mail: peter.kratzer@uni-due.de

Phone: +49 203 3793313. Fax: +49 203 3794732

**Abstract**

Various atomic structures for the interface between Au(111) and monolayers of $MoS_2$ and $MoSe_2$ are investigated by means of first-principles calculations approximating van der Waals interactions by pairwise atomic interactions. Calculated bond lengths and interface energies are reported. The focus is on calculation of vibrational spectra and their comparison to experimental data. The $MoSe_2$ monolayer, due to its almost perfect match with the Au(111) surface in the $(\sqrt{3} \times \sqrt{3})$R30° superstructure, shows shifts of less than one wavenumber of the Raman-active $A_{1g}$ and $E_{2g}$ vibrational modes upon physisorption on Au(111). For $MoS_2$, we find that two structural models, an almost unstrained superstructure with large periodicity, and a strained layer with $(\sqrt{3}\times\sqrt{3})$R30° supercell, may coexist, as evidenced by their almost identical formation energy. Considerable mode softening in the strained $MoS_2$ layer is observed, both in the $E^{(1)}_{2g}$ mode

*To whom correspondence should be addressed



Authors Accepted Manuscript

as a consequence of strain, but also in the $A_{1g}$ mode due to spill-over of charge from the Au(111) surface into the conduction band minimum of strained $MoS_2$. The latter observation helps to rationalize the experimentally observed satellite peak of the $A_{1g}$ Raman signal from $MoS_2$/Au(111) and other layered sulfides while this feature is absent in $MoSe_2$.

# Introduction

The interaction of two-dimensional (2D) materials with the substrate on which they are grown or onto which they have been transferred is a topic of considerable interest for the utilization of 2D materials in a wider technological context. For transition metal dichalcogenides (TMDC) such as e.g. $MoS_2$ and $MoSe_2$, growth on graphene as a substrate has been demonstrated both by MOVPE[1] and CVD.[2,3] Various approaches how to obtain large-area samples of TMDCs have been demonstrated.[4] However, one of the best ways to obtain such samples is still the exfoliation of TMDCs from bulk with the help of metallic surfaces, in particular gold surfaces.[5,6] In this paper, we report a computational study of the interaction of TMDCs, specifically $MoS_2$ and $MoSe_2$, with a gold substrate. This substrate is of particular interest since it interacts with TMDCs sufficiently strongly[5,7,8] (compared to chemically inert and/or insulating substrates, see e.g. Ref.s 3,9,10) while leaving the chemical structure of the TMDC intact. In addition to its role in exfoliation, the interface between TMDCs and metals surfaces is highly relevant for the formation of electronic contacts on TMDCs.[11–13]

Vibrational spectroscopies, and in particular Raman spectroscopy, are widely used experimental methods to characterize layers of 2D materials. Several factors, such as the number of atomic layers in the 2D film, the strain state and a possible electronic interaction with the substrate, give rise to shifts in the characteristic Raman-active modes. These shifts provide valuable information; it is, however, often difficult to disentangle the various contributions, both mechanical and electronic or chemical in nature, responsible for the shifts.

It is well known that bulk $MoS_2$ and $MoSe_2$ show characteristic Raman-active $E^{(1)}_{2g}$ and



Authors Accepted Manuscript

$A_{1g}$ modes located around 383 $cm^{-1}$ and 409 $cm^{-1}$ for $MoS_2$,[14] and around 286 $cm^{-1}$ and 242 $cm^{-1}$ for $MoSe_2$,[15] respectively. In thin films, symmetry selection rules determine which of the composite modes in multi-layered films are Raman active; hence this technique allows experimentalists to determine the number of layers in a film.[16,17] Moreover, shifts or splittings of the Raman peaks can provide information about the interaction between film and substrate. For $MoS_2$ films on gold, several experimental groups[7,8] have reported a downshift and a splitting of the $E^{(1)}_{2g}$ peak, whereas the $A_{1g}$ peak develops a satellite at lower frequency, slightly below 400 $cm^{-1}$. Already before, similar satellites had been observed for a $WS_2$ monolayer when covered with a thin gold layer.[18] For the $MoS_2$ monolayer, previous results for Au deposition had been indecisive: Some researchers reported only a strain-induced splitting of the $E^{(1)}_{2g}$ mode while the $A_{1g}$ mode remained virtually unaffected,[19] whereas another group reported even a stiffening of the $A_{1g}$ mode.[11] For $MoSe_2$ layers, however, the Raman modes appear to be unaffected[20] by the contact with gold.

The phonon dispersion in bulk $MoS_2$ is well known both from experiments[21] and, for few-layer films, from first-principles calculations.[22] The dependence of mode frequencies on strain has been studied experimentally using both uniaxially and biaxially strained samples.[23,24] While a clear lowering of the $E^{(1)}_{2g}$ mode frequency has been observed by all groups, the $A_{1g}$ mode showed a much weaker (or even vanishing) strain dependence. A qualitatively similar, but quantitatively larger down-shift of the $E^{(1)}_{2g}$ mode compared to previous work has been obtained by Conley *et al.*[25] In uniaxially strained samples, it is well documented that the doubly-degenerate $E^{(1)}_{2g}$ mode splits into two peaks. However, no such splitting under strain is expected nor observed in substrate-free strained films for the non-degenerate $A_{1g}$ mode. Thus, the satellites discussed above for TMDC monolayers on gold appear to be related not simply to mechanical strain, but in addition to some electronic or chemical interaction of the TMDCs with the gold substrate.

In this work, we performed first-principles calculations for several model structures of $MoS_2$/Au(111) and $MoSe_2$/Au(111) with particular interest in structural properties and



Authors Accepted Manuscript

vibrational spectra. By comparing the vibrational density of states of adsorbed and free-standing monolayers, we disentangle the contributions of both mechanical strain effects and electronic interaction effects to vibrational frequency shifts. We aim at identifying fingerprints in the vibrational spectra characteristic of adsorption and attempt to rationalize the recent experimental finding[8] of an additional Raman peak for $MoS_2$ adsorbed on gold. After reporting the computational details, we discuss the calculated vibrational spectra for both $MoS_2$ and $MoSe_2$ monolayers. Finally, we conclude by comparing the results among the two materials, as well as between theory and experiment.

## Computational Details

The aim of this work is the calculation of vibrational spectra for various geometries of $MoS_2$ and $MoSe_2$ monolayers on gold to make contact with experimental data from Raman spectroscopy. The geometries encountered in experiment may be non-ideal since the TMDC ML often consists of very small 'flakes', and the gold substrate is rarely a single-crystal surface. Moreover, the lattice parameters of $MoS_2$ and Au(111) do not match. For these reasons, we constructed three structural models (see Fig. 1): Model A uses a $1 \times 1$ unit cell and enforces a common lattice parameter of 3.08 Å on both $MoS_2$ and Au that resulted from a joint energy minimization of both the $MoS_2$ and the Au layers. This geometry could occur for a 'floating island' of Au adatoms on Au(111) that could adapt its lattice constant to come into registry with $MoS_2$, while at the same time the $MoS_2$ lattice is compressed by 4.4%. In model B, we use a $(\sqrt{13} \times \sqrt{13})$R13.9° supercell (see Ref. 26) for $MoS_2$ together with a $(4 \times 4)$ supercell for Au(111). As an advantage, this model almost completely avoids strain in both the substrate and the $MoS_2$ monolayer. However, it cannot account for the preferred orientation of $MoS_2$ flakes introduced by the frequently occurring $[\bar{1}10]$ and $[\bar{1}\bar{1}2]$-oriented steps on Au(111), since the monolayer is rotated by 13.9° with respect to the Au surface lattice. Finally, model C uses a $(\sqrt{3}\times\sqrt{3})$R30° supercell of $MoS_2$ that is brought into contact



Authors Accepted Manuscript

with a $(2 \times 2)$ supercell of Au(111). To retain the Au lattice constant, the $MoS_2$ layer had to be stretched by 4.1%. Model C allows for an alignment of the $[\bar{1}\bar{1}2]$ direction of the $MoS_2$ lattice with the $[\bar{1}10]$ direction on Au(111) (or vice versa) and thus could be suitable for describing the alignment of the $MoS_2$ flakes with steps on Au(111). In addition, we used this model to study pinning of the $MoS_2$ layer by a single-atom vacancy in Au(111). For $MoSe_2$, only model C was considered, since the slightly larger lattice parameter of $MoSe_2$ allows for an almost perfect lattice match with Au(111). For this material, models A and B would require a significant compression of $MoSe_2$ and are hence unlikely for energetic reasons.

All calculations in this paper were carried out within the density functional theory (DFT) framework using the VASP code,[27,28] with a plane wave cut-off energy of 550 eV. The ion-electron interaction was treated by means of the projector augmented wave method.[29] The generalized gradient approximation of Perdew, Burke, and Ernzerhof (PBE)[30] was used for the exchange-correlation functional. To take the van der Waals (vdW) interactions into account, a correction to the conventional Kohn-Sham DFT energy and forces was applied in the form of the dDsC dispersion correction proposed by Becke and Johnson.[31] We have chosen this scheme since we found it best suited to describe the interactions between TMDC layers in multilayer stacks, which could be important for future work addressing the phonon spectra of multilayers. For a comparison of the dDsC scheme to other pairwise correction methods, Ref.s 32,33 provides benchmark results for 2D materials. The vibrational frequencies and corresponding density of states (DOS) were calculated with the finite-displacement method using the Phonopy code.[34]

The Au(111) substrate is described by a slab consisting of five Au layers. In a first step, the positions of the atoms were optimized, thereby allowing for relaxations of the atoms in the TMDC layers and of the three topmost layers of the Au(111) slab, whereas the lattice parameter and the two bottom Au layers were held fixed in model B and C. These calculations yield the adsorption height that is crucially determined by the van der Waals interactions. The calculations of the phonon spectra have been performed twice, once for the



Authors Accepted Manuscript

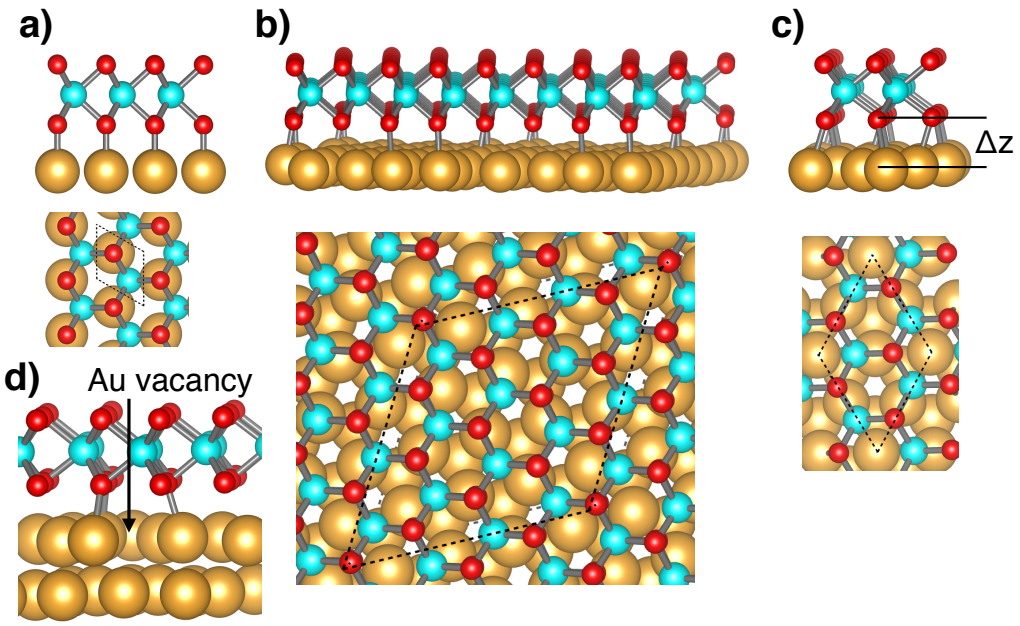


Figure 1: Ball-and-stick representation of a) model A b) model B, and c) model C. Both top view and side view are shown. d) side view of model C, but adsorbed on a Au(111) surface with one Au vacancy.

optimized geometry including the gold substrate, and once again for the free-standing TMDC layer frozen in the geometry that we had obtained by placing it on the substrate. By this procedure, we attempt to disentangle the mechanical effects resulting from the deformation from the electronic effects on the phonon spectrum resulting from charge transfer or orbital hybridization.

From the total energies obtained from the DFT calculations, the interface formation energy per formula unit can be obtained as

$$E_{\text{interface}} = (E_{\text{combined}} - E_{\text{Au}} - E_{\text{TMDC}})/N_{\text{Mo}}\,.$$

Here, $E_{\text{combined}}$ and $E_{\text{Au}}$ are the total energies of the combined system (TMDC plus Au(111) structurally optimized) and of the Au substrate kept frozen after lifting off the TMDC layer. $E_{\text{TMDC}}$ is the energy of a free-standing TMDC monolayer in which both the lattice constant and the atomic positions have been optimized, and $N_{\text{Mo}}$ is the number of Mo atoms in the



Authors Accepted Manuscript

structure.

# Results and Discussion

## $MoS_2$ monolayer

The interatomic distances for the three structural models are presented in Table 1. In all three models, Mo–S bond lengths are only slightly changed compared to an ideal free-standing monolayer. The distances $d_{\mathrm{Au-S}}$ between the sulfur atoms and the surface Au atoms are in the range of 2.51 to 2.79 Å, and thus much larger than the typical values of 2.0 to 2.1 Å for covalent bonds between S and Au, as encountered, for instance, when thiol groups are used to anchor organic molecules on Au surfaces.[35] While the shortest $d_{\mathrm{Au-S}}$ is found for the S atoms sitting on top of the Au atoms in model A, there are Au atoms in models B and C that do not have a direct S bonding partner; this leads to larger $d_{\mathrm{Au-S}}$ of 3.28 and 3.47 Å in models B and C. In addition to atomic distances, we also present the average distance $\Delta_z$ between the planes of surface Au atoms and S atoms of the lowest S layer in $MoS_2$. In models B and C, these are obtained by first averaging the heights of the S atoms and the $z$ positions of the Au surface layer atoms, and then forming the difference. For both these models, the interface formation energy $E_{\mathrm{interface}}(MoS_2/\mathrm{Au}(111)$ is found to be $-0.27$ eV per formula unit. The negative value indicates that it is energetically favorable for the $MoS_2$ layer to bind to the surface. A significant contribution to this binding energy stems from the van der Waals interaction. Note that a comparable value of the binding energy has been computed recently.[5] We conclude that, while the elastic strain energy in model C is an energetic cost, this is overcompensated by a somewhat stronger bonding to the gold surface. In total, the interface energy of the strained layer in model C is very close to the value for the almost unstrained model B.

For the $(1 \times 1)$ unit cell of model A, we considered two structures, one where the S atoms of the layer in contact with the substrate occupies the hcp hollow sites of Au(111), and one



Authors Accepted Manuscript

Table 1: Strain $\Delta a/a$ and interatomic distances (Å) calculated with the PBE+dDsC method for three structural models (cf. Fig. 1) of $MoS_2$/Au(111).

| | $\Delta a/a$ | $d^{\mathrm{min}}_{\mathrm{Au-S}}$ | $d^{\mathrm{max}}_{\mathrm{Au-S}}$ | $d_{\mathrm{Mo-S}}$ | $\Delta_z$ |
|---|---|---|---|---|---|
| model A | −4.4% | 2.51 | — | $2.384 \pm 0.001$ | 2.51 |
| model B | 0.15% | 2.74 | 3.28 | $2.416 \pm 0.005$ | 2.78 |
| model C | 4.1% | 2.79 | 3.47 | $2.44 \pm 0.01$ | 2.65 |

where S sits on top of the Au atoms. The latter one is the ground state that was considered further in the analysis of phonons, while the hcp hollow position was found to be only 0.003 eV higher in energy.

Model A has a unique value for the non-covalent Au–S bond length which amounts to 2.51 Å, whereas model B shows some variability: While the shortest Au–S distance is 2.74 Å, the longest is 3.28 Å. In model C, the Au–S distance is 2.79 Å, but one of the four Au atoms in the supercell has no S coordination partner. This Au atom, which is located in the center of a Mo–S-hexagon, is 3.47 Å away from the nearest S atom.

In addition, we used a $2\sqrt{3} \times 2\sqrt{3}$ unit cell to model adsorption of a $MoS_2$ monolayer on a Au(111) surface that contains one Au vacancy. After relaxing the Au substrate in the presence of the $MoS_2$ monolayer, we find that the Au surface atoms adjacent to the vacancy move slightly inward towards the vacancy. Due to this, their distance to other surface Au atoms is increased to 3.03 Å. The $MoS_2$ layer as a whole stays further away than at the perfect Au(111) surface. This shows up as an increased bond distance between some S and Au atoms of $d_{\mathrm{Au-S}} = 2.85 \pm 0.01$ Å, as compared to 2.79 Å in model C. Directly at the vacancy, however, sulphur atoms are more tightly bound, with a bonds length of 2.64 Å, to the Au atoms surrounding the Au vacancy (see Fig. 1d)). To adapt to the defective Au(111) surface, the $MoS_2$ monolayer has to bend slightly. This leads to a slight increase of the Mo–S bond length to a value of $d_{\mathrm{Mo-S}} = 2.45 \pm 0.02$ Å close to the Au vacancy, as compared to 2.44 Å in model C, and 2.416 Å in the nearly unstrained $MoS_2$ monolayer of model B. The overall bonding at the defective Au surface is larger by 0.59 eV per $2\sqrt{3} \times 2\sqrt{3}$ supercell compared to the prefect case in model C. Expressed per $MoS_2$ formula unit, the interface



Authors Accepted Manuscript

energy $E_{\text{interface}}$ changes slightly from $-0.27$ eV to $-0.32$ eV due to the presence of the Au vacancy. This enhanced binding energy may explain why in some experiments the lowest layer of a multi-layered $MoS_2$ flake appears to be immobile.

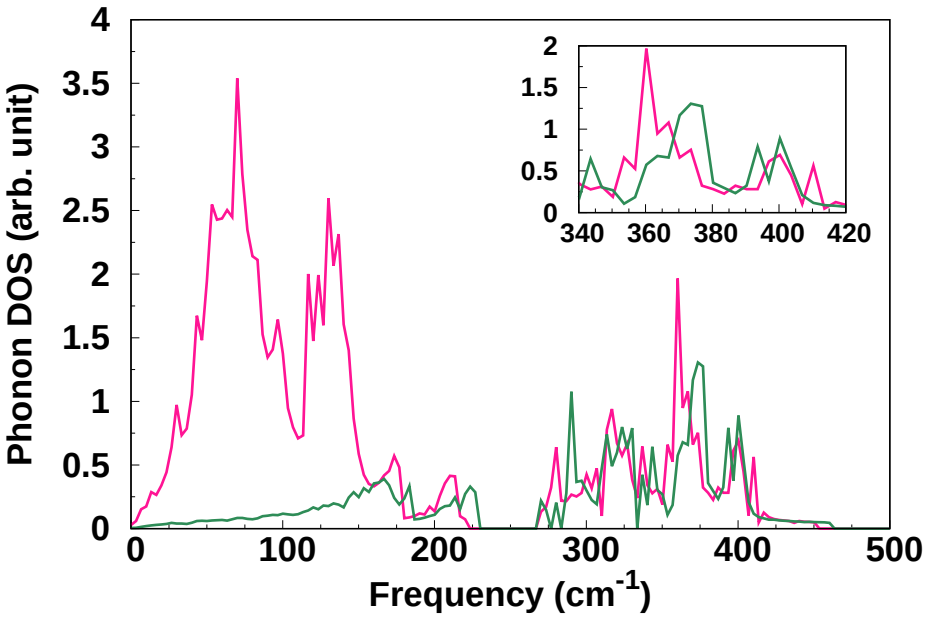


Figure 2: Phonon density of states of the $(\sqrt{13}\times\sqrt{13})$R13.9° $MoS_2$/Au(111) heterostructure (model B in Fig. 1b), pink line) and the corresponding $MoS_2$ monolayer without substrate (green line). The inset shows the region where the $A_1$ and E' modes are located.

The vibrational densities of state (vDOS) obtained from our calculations are displayed in Figs. 2, Fig. 4 and 3. For the $(\sqrt{13}\times\sqrt{13})$R13.9° structure, the strain in the $MoS_2$ layer is as small as 0.15%. The vibrational spectra of the $MoS_2$ layer on gold and of the structurally identical, but free-standing $MoS_2$ monolayer are very similar (Fig. 2). This tells us that the van der Waals interactions of $MoS_2$ with gold leave only small fingerprints, if any, in the vibrational structure. All modes below 150 $cm^{-1}$ have dominant gold character and are of little experimental relevance. We note that there is a shift of the peak in the vDOS at 210 $cm^{-1}$; this mode, corresponding a a zone-edge acoustic phonon of $MoS_2$, gets softer due to adsorption on the gold. The modes in this frequency range are not Raman active



Authors Accepted Manuscript

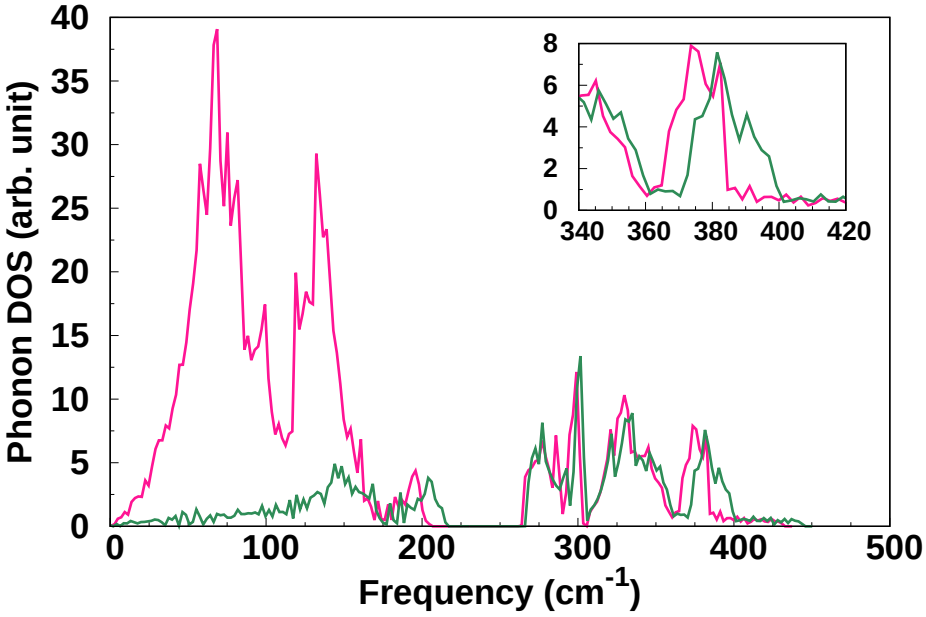


Figure 3: Phonon density of states of two types of $MoS_2$/Au(111) heterostructures compared: matched $(1 \times 1)$ (model A in Fig. 1a), green line) and $(\sqrt{13} \times \sqrt{13})$R13.9° structure (model B in Fig. 1, pink line). The inset shows the region where the $A_1$ and E' modes are located.

in extended structures and therefore difficult to probe experimentally. However, they are observed in nanostructures[36] and possibly in flakes where translation invariance is broken. The modes above 250 $cm^{-1}$ are due to optical phonons in the $MoS_2$ layer. Although these are not much affected by adsorption, there are subtle changes visible in the range between 300 and 410 $cm^{-1}$. This is also the frequency range usually probed experimentally by Raman spectroscopy.

Th effect of strain can best be studied by comparing the $(\sqrt{13} \times \sqrt{13})$R13.9° structure to the $(1 \times 1)$ unit cell that results from a 'forced match' between $MoS_2$ and gold which we called model A. Both vDOS are compared in Fig. 3. They shows similar gross features; however, all optical modes (at frequencies above 250 $cm^{-1}$) in the 'matched' $(1 \times 1)$ structure of $MoS_2$ are systematically shifted to higher frequencies. We attribute this finding to the compressive strain in the $MoS_2$ layer introduced by matching it to a common lattice constant



Authors Accepted Manuscript

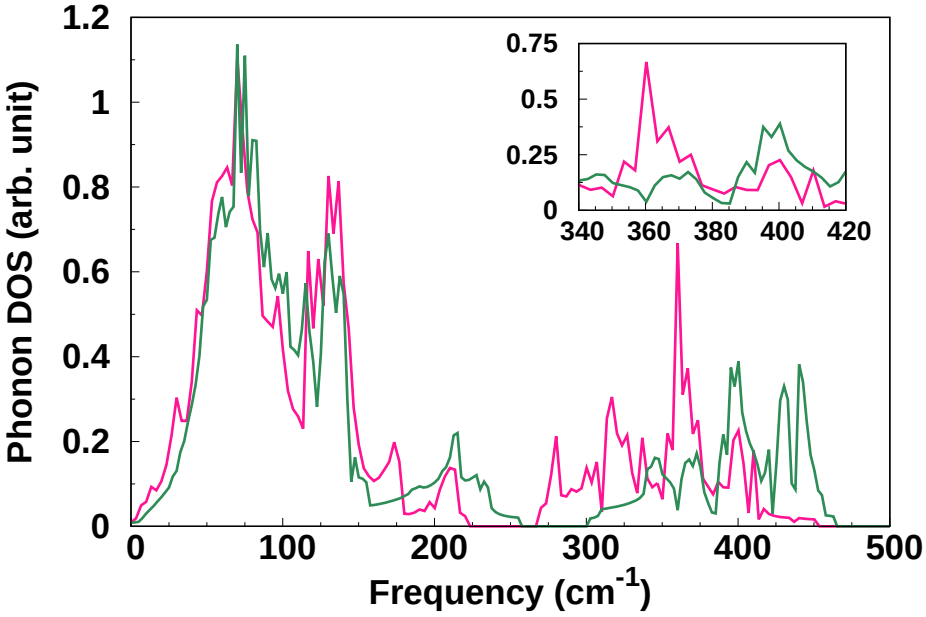


Figure 4: Phonon density of states of the $(\sqrt{3} \times \sqrt{3})$R30° $MoS_2$/Au(111) heterostructure (model C in Fig. 1c), pink line) and the corresponding $MoS_2$ monolayer without substrate (green line). The inset shows the region where the $A_1$ and E' modes are located.

with gold.

For the vDOS of the $(\sqrt{3} \times \sqrt{3})$ unit cell of model C shown in Fig. 4, we again observe a shifted peak due to the softened zone-boundary phonon near 200 $cm^{-1}$. In the frequency range of the optical phonons of $MoS_2$, the free-standing and the adsorbed monolayer show very similar vDOS with the exception of the highest peak around 400 $cm^{-1}$. The $A_{1g}$ mode of the free-standing film is shifted to lower wavenumber, below 400 $cm^{-1}$, if the layer is adsorbed on Au(111). The reason for this softening will be discussed below.

For a quantitative analysis of peak shifts, we inspected the phonon band structures in addition to the vDOS. In the literature, the nomenclature of the modes often follows the conventions for the bulk structure with $D_{6h}$ symmetry, i.e. one speaks of the $E_{2g}$ and $A_{1g}$ modes, while it is more correct to speak of the E' and $A_1$ modes in case of a monolayer with $D_{3h}$ symmetry. Since Raman spectroscopy has its highest sensitivity to modes near



Authors Accepted Manuscript

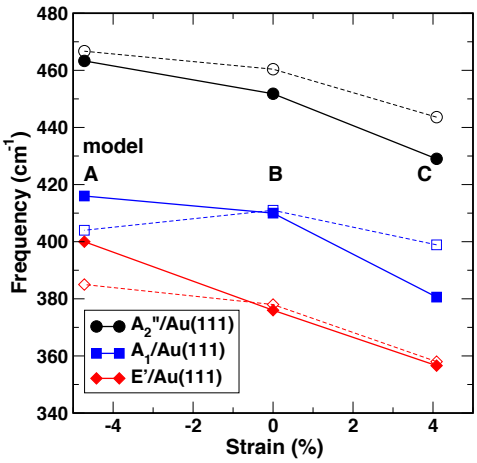


Figure 5: Dependence of vibrational wavenumbers of the $MoS_2$ monolayer on Au(111) on strain, extracted from the three models A, B and C presented in Fig. 1. The full symbols are for the optimized atomic structure on Au(111), the open symbols are for the same structure, but free-standing without substrate.

the Γ point of the Brillouin zone, we use vibrational frequencies of Γ-point phonons for the quantitative comparison shown in Fig. 5. The highest mode, the $A_2^{"}$ mode, is not Raman active, but is easily identifiable as the topmost band in the phonon band structures. For the $A_1$ and the E' modes, some caution is required when analyzing the supercell calculations to distinguish the original modes from phonon branches resulting from backfolding. Since the $A_1$ band is dispersing upward to higher frequencies, we report the band bottom, whereas the top of the phonon band is reported for the (two-fold degenerate at Γ) band of the E' mode. The wavenumbers of these modes are collected in Table 2. The results for all three models are collected and plotted in Fig. 5 as function of the mismatch of lattice constants between the $MoS_2$ superstructure and the Au(111) surface layer.

As can be seen from Fig. 5, the frequency of the $A_2^{"}$ and E' modes are generally lowered by the presence of tensile strain, both in the free-standing and in the Au-supported monolayers. This trend is in agreement with previous findings both in the experimental and computational studies. For the $A_1$ mode of the free-standing films, we see no clear trend for the strain dependence from our calculations. However, for the Au-supported monolayers, a softening of the $A_1$ mode with increasing strain is observed. In particular, the tensile strain in the



Authors Accepted Manuscript

structural model C reduces the $A_1$ vibrational wavenumber to 380.6 $cm^{-1}$.

The physical reason for this unusual mode softening can be traced back to the electronic structure. The tensile strain in the $MoS_2$ layer leads to an energetic down-shift of the $MoS_2$ conduction band. As a result, a spill-over of electronic charge from electronic states at the gold surface into $MoS_2$ conduction band states becomes possible. This interpretation is supported by an analysis of the orbital projected electronic density of states displayed in Fig. 6. The Fermi energy of gold comes to lie in the lower tail of the $MoS_2$ conduction band states contributed by $4d$ orbitals of the Mo atoms. Population of these orbitals makes an anti-bonding contribution to the Mo–S bonds. This shows up as an increased bond length $d_{\mathrm{Mo-S}} = 2.44$Å as compared to 2.416Å in the unstrained $MoS_2$ layer, cf. Table 1. Even if the bond elongation is moderate, the frequency of the $A_1$ mode is quite sensitive to this change in electronic structure. A lowering of the $A_{1g}$ mode frequency due to charge doping has been reported previously by Frey *et al.*[36] and by Chakraborty *el al.*[37] These authors argued that the conduction band edge in monolayer TMDCs has the character of the $4d_{z^2}$ orbital of the Mo atom, and thus belongs to the same symmetry representation as the $A_{1g}$ mode. Therefore, population or hybridization of this orbital with electronic states of the Au surface may have a notable effect on the stiffness of this mode. The symmetry argument also explains why the degenerate $E_{2g}$ modes that involve atomic motions of the S atoms parallel to the layer show only little sensitivity to charging effects, since their representation is orthogonal to the $e_g$ representation to which the $4d_{z^2}$ orbital belongs.

Experimentally, the Raman spectra of $MoS_2$ flakes on gold substrates are found to display two Raman peaks at 397 and above 400 $cm^{-1}$, whereas no signal has been observed above 450 $cm^{-1}$.[3] The absence of such a high-lying mode indicates that the van der Waals interaction with the gold substrate is not able to enforce a large compression onto the $MoS_2$ lattice, as would be required for model A. The experimentally observed splitting of the $A_1$ peak could be explained by a coexistence of model B and C that are realized locally on different spots at the surface. According to our calculations, this would give rise to a lower



Authors Accepted Manuscript

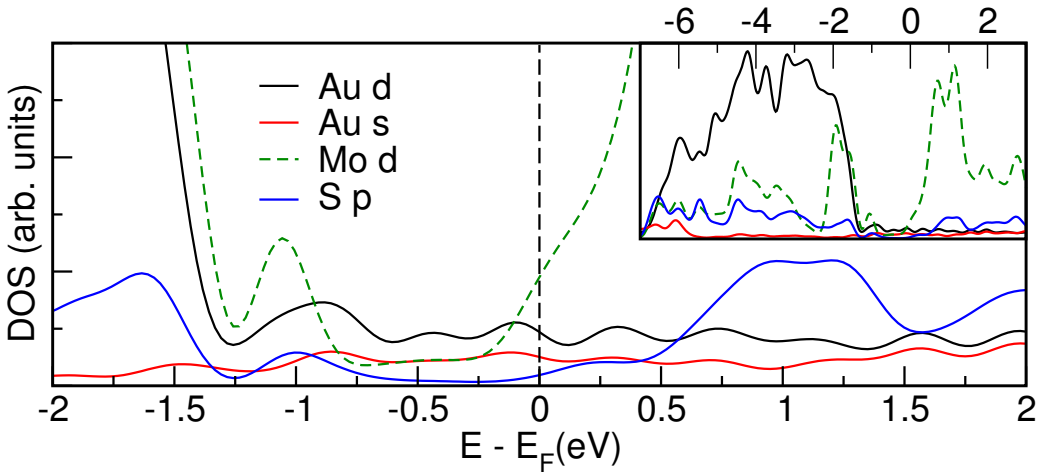


Figure 6: Electronic density of states (DOS) of the $(\sqrt{3} \times \sqrt{3})$R30° $MoS_2$/Au(111) heterostructure, model C in Fig. 1c). The Fermi level is chosen as the zero of energy. The 4d orbitals of Mo forming the conduction band of the strained $MoS_2$ monolayer develop a low-energy tail reaching down below the Fermi level. The inset shows the DOS over a wider energy range.

and an upper $A_1$-related peak at 381 and 410 $cm^{-1}$, respectively. While the tensile strain in the $MoS_2$ layer present in model C is certainly an energetic cost, this model may still be realized close to Au surface vacancies (see the structural model discussed above) or near steps of the Au(111) surface. In both cases, a specific spatial arrangement of the S atoms with respect to undercoordinated surface Au atoms is required to pick up some covalent contribution to the Au–S bond which is hardly present for the fully coordinated Au atoms of a perfect Au(111) surface. This constraint may enforce a specific local orientation and/or strain state of the $MoS_2$ flake which resembles model C and thus, via the spill-over of charge, leads to the low-frequency satellite of the $A_1$ peak.

## $MoSe_2$ monolayer

Because of the much closer match of the lattice constants of $MoSe_2$ in a $\sqrt{3} \times \sqrt{3}$ structure with the $(2 \times 2)$ Au(111) supercell, we solely considered this possibility, termed model C above, for the adsorption of $MoSe_2$ on Au(111). After structure optimization, the bond length of Se to the closest Au atom is found to be $d_{\mathrm{Au-Se}} = 3.03$Å . Within the adsorbed



Authors Accepted Manuscript

monolayer, Mo–Se bonds are 2.54Å in length. This may be compared to the Mo–Se bond length of 2.54Å in a fully optimized, free-sanding monolayer, indicating that the interface formation is free of strain. The interface energy is computed as 0.48 eV per formula unit of $MoSe_2$, somewhat larger than for $MoS_2$.

Since the strain due to the mismatch of lattice constants between $MoSe_2$ and Au(111) is just 0.4 %, the vibrational frequencies of the $MoSe_2$ monolayer on Au(111) are rather close to those of a free-standing $MoSe_2$ monolayer (see Fig. 7). Due to the larger mass of the Se atoms compared to S atoms, the relative positions of the vibrational modes are interchanged in $MoSe_2$ and $MoS_2$. In particular, the Raman-active $A_1$ mode appears at lower wavenumber than the E' mode in $MoSe_2$, in contrast to $MoS_2$ where the $A_1$ mode is higher in wavenumber. Experimentally, the $A_1$ mode has been detected[38] at 240 $cm^{-1}$ or 241 $cm^{-1}$,[39] while 287.5 $cm^{-1}$ had been reported[39] for the E' mode. These values agree with the vibrations in bulk within 1 $cm^{-1}$. In our calculations (cf. Table 2), we obtain 236.2 $cm^{-1}$ for the $A_1$ mode of $MoSe_2$ adsorbed on Au(111), while 235.8 $cm^{-1}$ is obtained in the same (frozen) $MoSe_2$ structure lifted off from the substrate. For the E' mode, the corresponding values are 281.8 $cm^{-1}$ on Au(111), and 282.7 $cm^{-1}$ in the free-standing structure. Thus, it is clear that the electronic effect of the substrate is much smaller in the $MoSe_2$ monolayer than in the $MoS_2$ monolayer. While the absolute values in our calculations are systematically about 5 $cm^{-1}$ lower than the experimental values, experiment[20] and our theory agree in the negligibly small shift ($< 1$ $cm^{-1}$) caused by adsorption on Au(111).

Table 2: Wavenumber ($cm^{-1}$) of $A_{1g}$ and $E^{(1)}_{2g}$ modes for the $\sqrt{3} \times \sqrt{3}$ structure (model C) of $MoS_2$ and $MoSe_2$ on Au(111). The values for the adsorbed monolayer and for a free-standing monolayer with the same structure are compared.

| symmetry | | $MoS_2$ | | $MoSe_2$ | |
|---|---|---|---|---|---|
| $D_{3h}$ | $D_{6h}$ | on Au(111) | free | on Au(111) | free |
| $A_1$ | $A_{1g}$ | 380.6 | 399.0 | 236.2 | 235.8 |
| E' | $E^{(1)}_{2g}$ | 356.6 | 358.0 | 281.8 | 282.7 |



Authors Accepted Manuscript

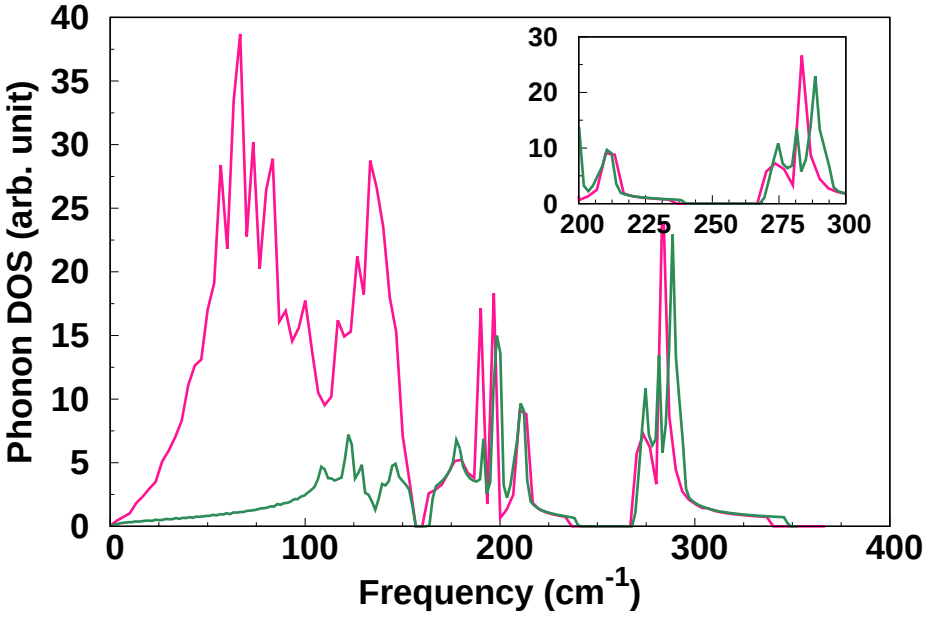


Figure 7: Phonon density of states of the $\sqrt{3} \times \sqrt{3}$R30° $MoSe_2$/Au(111) heterostructure (pink line) and the corresponding $MoSe_2$ monolayer without substrate (green line). The inset shows the region where the $A_1$ and E' modes are located.

# Conclusion

In summary, we find from density-functional theory (DFT) calculations including a pairwise correction term for the van der Waals interaction that the distance between a gold substrate and a monolayer of TDMCs is in the range of 2.5 to 2.8Å for $MoS_2$, and about 3.03Å for $MoSe_2$. These findings point to the dominant role of van der Waals bonding in TMDCs on a noble metal surface, with a moderate covalent contribution if sulphur attaches to an undercoordinated Au atom, e.g. close to a Au surface vacancy. Consequently, one expects only small effects due to the TMDC - surface interaction in the vibrational Raman spectra of the TMDCs, in particular for $MoSe_2$ for which a good lattice match between Au(111) and $MoSe_2$ can be obtained in the $(\sqrt{3} \times \sqrt{3})$R30° superstructure. For $MoS_2$, the shift of the $E^{(1)}_{2g}$ mode to lower frequencies upon adsorption can be explained by mechanical strain



Authors Accepted Manuscript

in the $MoS_2$ layer that may occur near point defects or steps of the Au(111) surface. The calculations show that tensile strain on $MoS_2$ leads to a lowering of its conduction band and partial population of this band due to electronic spill-over from the Au surface. Since the $A_{1g}$ mode is particularly sensitive to such a charge transfer effect, a distinct lowering of the $A_{1g}$ mode to frequencies below 400 $cm^{-1}$ occurs in strained regions. This is corroborated by DFT calculations with a $(\sqrt{3} \times \sqrt{3})R30°$ supercell of $MoS_2$/Au(111) with a strain of 4.1%. In view of these results, a coexistence of strained and unstrained areas of the $MoS_2$ layer on Au(111) is the most likely explanation of the experimental observation of the splitting of the $A_{1g}$ mode into a main peak and a lower satellite peak shortly below 400 $cm^{-1}$. For $MoSe_2$, such a satellite is neither expected nor observed, in line with the very low strain in the $MoSe_2$/Au(111) superstructure. As a fingerprint of adsorption, a softening of the acoustic zone-boundary modes is predicted by our calculations for both $MoS_2$ and $MoSe_2$ on gold. However, this mode is accessible to Raman spectroscopy only if translational symmetry is broken.

## Acknowledgement

The authors gratefully acknowledge the Gauss Centre for Supercomputing e.V. (www.gauss-centre.eu) for funding this project by providing computing time through the John von Neumann Institute for Computing (NIC) on the GCS Supercomputer JUWELS at Jülich Supercomputing Centre (JSC). Financial support within SFB 1242 "Non-equilibrium dynamics of condensed matter in the time domain" funded by Deutsche Forschungsgemeinschaft (DFG), project number 278162697, is gratefully acknowledged. We thank Erik Pollmann and Marika Schleberger for helpful discussions on their experimental findings.

## References

(1) Grundmann, A.; McAleese, C.; Conran, B.; Pakes, A.; Andrzejewski, D.; Kümmell, T.; Bacher, G.; Teo, K.; Heuken, M.; Kalisch, H.; Vescan, A. MOVPE of Large-Scale



Authors Accepted Manuscript

$MoS_2/WS_2$, $WS_2/MoS_2$, $WS_2$/Graphene and $MoS_2$/Graphene 2D-2D Heterostructures for Optoelectronic Applications. *MRS Adv.* **2020**, *5*, 1625–1633.

(2) Cai, Z.; Liu, B.; Zou, X.; Cheng, H.-M. Chemical Vapor Deposition Growth and Applications of Two-Dimensional Materials and Their Heterostructures. *Chem. Rev.* **2018**, *118*, 6091–6133.

(3) Pollmann, E.; Morbec, J. M.; Madauß, L.; Bröckers, L.; Kratzer, P.; Schleberger, M. Molybdenum Disulphide Nanoflakes Grown by Chemical Vapour Deposition on Graphite: Nucleation, Orientation, and Charge Transfer. *J. Phys. Chem. C* **2020**, *124*, 2689 – 2697.

(4) Zavabeti, A.; Jannat, A.; Zhong, L.; Haidry, A. A.; Yao, Z.; Ou, J. Z. Two-Dimensional Materials in Large Areas: Synthesis, Properties and Applications. *Nano-Micro Lett.* **2020**, *12*, 66.

(5) Velický, M.; Donnelly, G. E.; Hendren, W. R.; McFarland, S.; Scullion, D.; DeBenedetti, W. J. I.; Correa, G. C.; Han, Y.; Wain, A. J.; Hines, M. A. et al. Mechanism of Gold-Assisted Exfoliation of Centimeter-Sized Transition-Metal Dichalcogenide Monolayers. *ACS Nano* **2018**, *12*, 10463–10472.

(6) Huang, Y.; Pan, Y.-H.; Yang, R.; Bao, L.-H.; Meng, L.; Luo, H.-L.; Cai, Y.-Q.; Liu, G.-D.; Zhao, W.-J.; Zhou, Z.; et al. Universal Mechanical Exfoliation of Large-Area 2D Crystals. *Nat. Commun.* **2020**, *11*, 2453.

(7) Velický, M.; Rodriguez, A.; Bouša, M.; Krayev, A. V.; Vondráček, M.; Honolka, J.; Ahmadi, M.; Donnelly, G. E.; Huang, F.; Abruña, H. D.; et al. Strain and Charge Doping Fingerprints of the Strong Interaction between Monolayer $MoS_2$ and Gold. *J. Phys. Chem. Lett.* **2020**, *11*, 6112–6118.

(8) Pollmann, E.; Sleziona, S.; Foller, T.; Hagemann, U.; Gorynski, C.; Petri, O.; Madauß, L.; Breuer, L.; Schleberger, M. Large-Area, Two-Dimensional $MoS_2$ Exfoli-



Authors Accepted Manuscript

ated on Gold: Direct Experimental Access to the Metal-Semiconductor Interface. *ACS Omega* **2021**, *6*, 15929.

(9) Shree, S.; George, A.; Lehnert, T.; Neumann, C.; Benelajla, M.; Robert, C.; Marie, X.; Watanabe, K.; Taniguchi, T.; Kaiser, U.; Urbaszek, B.; Turchanin, A. High Optical Quality of $MoS_2$ Monolayers Grown by Chemical Vapor Deposition. *2D Mater.* **2019**, *7*, 015011.

(10) Pollmann, E.; Madauß, L.; Schumacher, S.; Kumar, U.; Heuvel, F.; vom Ende, C.; Yilmaz, S.; Güngörmüs, S.; Schleberger, M. Apparent Differences between Single Layer Molybdenum Disulphide Fabricated via Chemical Vapour Deposition and Exfoliation. *Nanotechnol.* **2020**, *31*, 505604.

(11) Gong, C.; Huang, C.; Miller, J.; Cheng, L.; Hao, Y.; Cobden, D.; Kim, J.; Ruoff, R. S.; Wallace, R. M.; Cho, K.; Xu, X.; Chabal, Y. J. Metal Contacts on Physical Vapor Deposited Monolayer $MoS_2$. *ACS Nano* **2013**, *7*, 11350–11357.

(12) Pan, Y.; Li, S.; Ye, M.; Quhe, R.; Song, Z.; Wang, Y.; Zheng, J.; Pan, F.; Guo, W.; Yang, J.; Lu, J. Interfacial Properties of Monolayer $MoSe_2$ - Metal Contacts. *J. Phys. Chem. C* **2016**, *120*, 13063–13070.

(13) Kahnouji, H.; Kratzer, P.; Hashemifar, S. J. Ab initio Simulation of the Structure and Transport Properties of Zirconium and Ferromagnetic Cobalt Contacts on the Two-Dimensional Semiconductor $WS_2$. *Phys. Rev. B* **2019**, *99*, 035418.

(14) Wieting, T. J.; Verble, J. L. Infrared and Raman Studies of Long-Wavelength Optical Phonons in Hexagonal $MoS_2$. *Phys. Rev. B* **1971**, *3*, 4286–4292.

(15) Sekine, T.; Izumi, M.; Nakashizu, T.; Uchinokura, K.; Matsuura, E. Raman Scattering and Infrared Reflectance in 2H-$MoSe_2$. *J. Phys. Soc. Japan* **1980**, *49*, 1069–1077.



Authors Accepted Manuscript

(16) Scheuschner, N.; Gillen, R.; Staiger, M.; Maultzsch, J. Interlayer Resonant Raman Modes in Few-Layer $MoS_2$. *Phys. Rev. B* **2015**, *91*, 235409.

(17) O'Brian, M.; McEvory, N.; Hanlon, D.; Hallam, T.; Coleman, J. N.; Duesberg, G. S. Mapping of Low-frequency Raman Modes in CVD-Grown Transition Metal Dichalcogenides: Layer Number, Stacking Orientation and Resonant Effects. *Sci. Rep.* **2015**, *6*, 19476.

(18) Zhao, W.; Wu, Q.; Hao, Q.; Wang, J.; Li, M.; Zhang, Y.; Bi, K.; Chan, Y.; Ni, Z. Plasmon-Phonon Coupling in Monolayer $WS_2$. *Appl. Phys. Lett.* **2016**, *108*, 131903.

(19) Sun, Y.; Liu, K.; Hong, X.; Chen, M.; Kim, J.; Shi, S.; Wu, J.; Zettl, A.; Wang, F. Probing Local Strain at $MX_2$–Metal Boundaries with Surface Plasmon-Enhanced Raman Scattering. *Nano Lett.* **2014**, *14*, 5329–5334.

(20) Abid, I.; Chen, W.; Yuan, J.; Najmaei, S.; Peñafiel, E. C.; Péchou, R.; Large, N.; Lou, J.; Mlayah, A. Surface Enhanced Resonant Raman Scattering in Hybrid $MoSe_2$@Au Nanostructures. *Opt. Express* **2018**, *26*, 29411–29423.

(21) Tornatzky, H.; Gillen, R.; Uchiyama, H.; Maultzsch, J. Phonon Dispersion in $MoS_2$. *Phys. Rev. B* **2019**, *99*, 144309.

(22) Molina-Sanchez, A.; Wirtz, L. Phonons in Single-Layer and Few-Layer $MoS_2$ and $WS_2$. *Phys. Rev. B* **2011**, *84*, 155413.

(23) Lloyd, D.; Liu, X.; Christopher, J. W.; Cantley, L.; Wadehra, A.; Kim, B. L.; Goldberg, B. B.; Swan, A. K.; Bunch, J. S. Band Gap Engineering with Ultralarge Biaxial Strain in Suspended Monolayer $MoS_2$. *Nano Lett.* **2016**, *16*, 5836.

(24) Rice, C.; Young, R. J.; Zan, R.; Bangert, U.; Wolverson, D.; Georgiou, T.; Jalil, R.; Novoselov, K. S. Raman-Scattering Measurements and First-Principles Calculations of Strain-Induced Phonon Shifts in monolayer $MoS_2$. *Phys. Rev. B* **2013**, *87*, 081307.



Authors Accepted Manuscript

(25) Conley, H. J.; Wang, B.; Ziegler, J. I.; Haglund Jr., R. F.; Pantelides, S. T.; Bolotin, K. I. Bandgap Engineering of Strained Monolayer and Bilayer $MoS_2$. *Nano Lett.* **2013**, *13*, 3626 – 3630.

(26) Bruix, A.; Miwa, J. A.; Hauptmann, N.; Wegner, D.; Ulstrup, S.; Grønborg, S. S.; Sanders, C. E.; Dendzik, M.; Grubišić Čabo, A.; Bianchi, M.; Lauritsen, J. V.; Khajetoorians, A. A.; Hammer, B.; Hofmann, P. Single-layer $MoS_2$ on Au(111): Band Gap Renormalization and Substrate Interaction. *Phys. Rev. B* **2016**, *93*, 165422.

(27) Kresse, G.; Furthmüller, J. Efficient Iterative Schemes for ab initio Total Energy Calculations Using a Plane-Wave Basis Set. *Phys. Rev. B* **1996**, *54*, 11169–11186.

(28) Kresse, G.; Joubert, D. From Ultrasoft Pseudopotentials to the Projector Augmented-Wave Method. *Phys. Rev. B* **1999**, *59*, 1758 – 1775.

(29) Blöchl, P. Projector Augmented-Wave Method. *Phys. Rev. B* **1996**, *50*, 17953 – 17979.

(30) Perdew, J. P.; Burke, K.; Ernzerhof, M. Generalized Gradient Approximation Made Simple. *Phys. Rev. Lett.* **1996**, *77*, 3865–3868.

(31) Becke, A. D.; Johnson, E. R. Exchange-Hole Dipole Moment and the Dispersion Interaction Revisited. *J. Chem. Phys.* **2007**, *127*, 154108.

(32) Tawfik, S. A.; Gould, T.; Stampfl, C.; Ford, M. J. Evaluation of van der Waals Density Functionals for Layered Materials. *Phys. Rev. Mater.* **2018**, *2*, 034005.

(33) Björkman, T.; Gulans, A.; Krasheninnikov, A. V.; Nieminen, R. M. van der Waals Bonding in Layered Compounds from Advanced Density-Functional First-Principles Calculations. *Phys. Rev. Lett.* **2012**, *108*, 235502.

(34) Togo, A.; Tanaka, I. First-Principles Phonon Calculations in Materials Science. *Scr. Mater.* **2015**, *108*, 1 – 5.



Authors Accepted Manuscript

(35) Hekele, J.; Linke, M.; Keller, T.; Jose, J.; Hille, M.; Hasselbrink, E.; Schlücker, S.; Kratzer, P. A Fresh Look at the Structure of Aromatic Thiol on Au Surfaces From Theory and Experiment. *J. Chem. Phys.* **2021**, *155*, 044707.

(36) Frey, G. L.; Tenne, R.; Matthews, M. J.; Dresselhaus, M. S.; Dresselhaus, G. Raman and Resonance Raman Investigation of $MoS_2$ Nanoparticles. *Phys. Rev. B* **1999**, *60*, 2883–2892.

(37) Chakraborty, B.; Bera, A.; Muthu, D. V. S.; Bhowmick, S.; Waghmare, U. V.; Sood, A. K. Symmetry-Dependent Phonon Renormalization in Monolayer $MoS_2$ Transistor. *Phys. Rev. B* **2012**, *85*, 161403.

(38) Tonndorf, P.; Schmidt, R.; Böttger, P.; Zhang, X.; Börner, J.; Liebig, A.; Albrecht, M.; Kloc, C.; Gordan, O.; Zahn, D. R. T. et al. Photoluminescence Emission and Raman Response of Monolayer $MoS_2$, $MoSe_2$ and $WSe_2$. *Opt. Express* **2013**, *21*, 4908 – 4916.

(39) Kim, K.; Lee, J.; Nam, D.; Cheong, H. Davidov Splitting and Excitonic Resonance Effects in Raman Spectra of Few-Layer $MoSe_2$. *ACS Nano* **2016**, *10*, 8113 – 8120.



Authors Accepted Manuscript

# Graphical TOC Entry

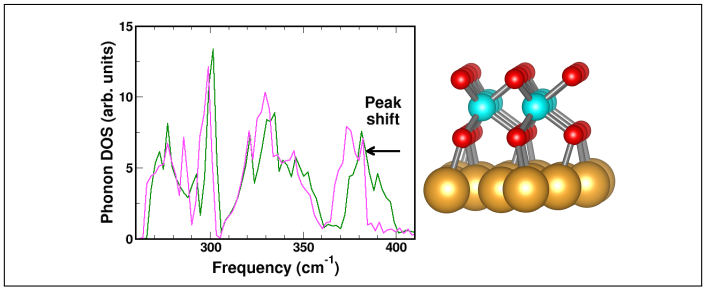




Authors Accepted Manuscript

DuEPublico

Duisburg-Essen Publications online

UNIVERSITÄT DUISBURG ESSEN

Offen im Denken

ub | universitäts bibliothek

This text is made available via DuEPublico, the institutional repository of the University of Duisburg-Essen. This version may eventually differ from another version distributed by a commercial publisher.

**DOI:** 10.1021/acs.jpcc.1c08594
**URN:** urn:nbn:de:hbz:465-20230905-112214-1

This document is the **Accepted Manuscript** version of a Published Work that appeared in final form in: *Journal of Physical Chemistry C : Nanomaterials and Interfaces*, 2021, 125, 48, 26645–26651, Copyright © American Chemical Society after peer review and technical editing by the publisher. To access the final edited and published work see https://doi.org/10.1021/acs.jpcc.1c08594.

All rights reserved.